Int. J. Heat Mass Transfer. Vol. 34, No. 12, pp. 3061–3074, 1991
Printed in Great Britain

0017–9310/91 $3.00 + 0.00
Pergamon Press plc

Numerical and experimental study of multicellular free convection flows in an annular porous layer

M. C. CHARRIER-MOJTABI
University of Paris VI, Place Jussieu, 75005 Paris, France

A. MOJTABI
Laboratoire de Mécanique, University of Toulouse III,
I.M.F.T., Avenue du Pr. Camille Soula, 31400 Toulouse, France

and

M. AZAIEZ and G. LABROSSE
L.I.M.S.I., University of Paris XI, Campus Universitaire, 91405 Orsay Cedex, France

(*Received* 30 *July* 1990 *and in final form* 3 *December* 1990)

Abstract—A numerical and experimental study of free convection two-dimensional (2D) flows in a saturated porous horizontal annulus is reported. The fluid motion, described by 2D Darcy–Boussinesq equations, is obtained from two different numerical methods, namely Fourier–Galerkin and collocation–Chebyshev methods, for high approximations. A comparison of the spectral accuracy of these two methods is carried out. Numerical results indicate that the collocation–Chebyshev method gives a better accuracy especially for the description of the boundary layers developed near the inner and outer cylinders. An experimental study using the Christiansen effect for the visualization of the thermal fields shows the existence of bicellular 2D structures. These structures, which have never been previously observed for concentric cylinders and by means of the Christiansen effect, are in good agreement with numerical results.

1. INTRODUCTION

THE STUDY of natural convection, in a porous layer bounded by two horizontal isothermal concentric cylinders, has a wide variety of technological applications ranging from thermal insulators such as gas-lines in gas-cooled reactors, cryogenics, underground cable systems, storage of thermal energy, etc.

The problem of accurately determining the fluid flow and heat transfer fields has proved to be quite challenging and has stimulated a large number of investigations over the past 20 years.

The main results concern the numerical study of the two-dimensional (2D) steady state which appears in the porous layer for low Rayleigh numbers. Several approaches have been developed such as the finite difference method and the perturbation method (Caltagirone [1] with ADI method, Burns and Tien [2] with SOR method), the finite element method (Mojtabi *et al.* [3]) and the Galerkin spectral method (Charrier-Mojtabi and Caltagirone [4], Rao *et al.* [5], Himasekhar and Bau [6]). These authors [4–6] expanded the temperature and the stream function with truncated Fourier series with orders of approximation less than 20×20 (in the r- and ϕ-directions, respectively).

Taking into account the radiative effect, Echigo *et al.* [7] studied the 2D steady state using a finite difference method. Bau [8] with a perturbation method, analysed the effect of eccentricity on the overall heat transfer rate. Himasekhar and Bau [9] used a boundary-layer technique and determined a correlation law between the Nusselt number, the Rayleigh number, the radii ratio and the eccentricity for an eccentric annulus and large Rayleigh numbers.

Caltagirone [1] proposed a three-dimensional (3D) numerical analysis using a finite element method but no significant results have been obtained to explain the experimentally observed flow pattern. Fukuda *et al.* [10] obtained 3D results using a finite difference method (SOR) for inclined annuli, but these results could not be extended to the horizontal case due to the presence of the gravitational force axial component direction which does not exist in a horizontal annulus. Charrier-Mojtabi *et al.* [11] used a 3D Galerkin scheme expanding the temperature and the velocity fields into truncated Fourier series, but only low orders of approximation have been considered. More recently, Rao *et al.* [12] have developed the temperature and the potential vector fields into Fourier series with orders of approximation up to $10 \times 13 \times 5$ (in the r-, ϕ-, and z-directions, respectively). For all these 3D studies, the authors assume that the flow is symmetrical with respect to a vertical plane including the cylinder's axis. According to the experiments, this assumption is valid for the 2D state. However, for the 3D study, this assumption may reduce the generality of the problem.

NOMENCLATURE

g	gravitational acceleration
K	permeability of the porous medium
L	axial length of the cell
Nu_g^*	average Nusselt number
r_i, r_o	inner and outer cylinder radii
r'	radial distance
r	coordinate in radius direction scaled by r_i
R	ratio of the outer to the inner radius
Ra^*	Rayleigh number, $g\beta K(T_i - T_o)r_i(\rho c)_f/(\lambda^* \nu)$
T'	temperature
T	dimensionless temperature, $(T' - T_o)/(T_i - T_o)$
T_i, T_o	inner and outer cylinder temperatures
t	dimensionless time
X	transformed coordinate, $\ln r$
Y	transformed coordinate, ϕ.

Greek symbols

α	$1/\ln(R)$
β	thermal expansion coefficient of the fluid
ε	porosity of the porous medium
λ^*	equivalent thermal conductivity of the saturated porous medium
ν	kinematic viscosity of the fluid
$(\rho c)_f$	heat capacity of the fluid
ϕ	angular coordinate
ψ	stream function.

Subscripts

i	inner
o	outer
′	real variables.

Stability studies have been carried out in refs. [1, 6]. Caltagirone [1] has studied the transition between the steady unicellular 2D state and the 3D state, Himasekhar and Bau [6] have proposed a linear stability analysis of the multicellular 2D flows with 2D perturbations localized in the basic flow plane.

Experimental studies about this subject were first developed by Cloupeau and Klarsfeld [13] using the Christiansen effect to visualize the thermal fields corresponding to the unicellular 2D flows. Caltagirone [1] has determined, by means of temperature measurements, the critical Rayleigh number for the transition between the unicellular 2D flow and the 3D flow pattern. Bau *et al.* [14] have observed 2D multicellular structure in a Hele–Shaw cell for an eccentric annulus, but this multicell structure turned out to be unstable and became unicellular after a period of time.

In the present study, the accuracy of the Fourier–Galerkin spectral method is analysed, especially for the representation of the multicellular 2D flows which appear for high Rayleigh numbers. Orders of approximation up to 50×50 are considered. However, the spectral convergence of this method is not satisfactory; so a new representation of the solution using a collocation–Chebyshev approximation, in the radial (confined) direction, is developed and a comparison between these two numerical methods is carried out. In order to prove the physical existence of multicellular 2D flows, obtained numerically, several experiments have been made, using the Christiansen effect to visualize the thermal fields. The experimental conditions inducing the apparition of the bicellular flow are investigated with particular attention.

2. THE NUMERICAL APPROACH

2.1. *The 2D problem formulation*

Let us consider a porous annular region bounded by two horizontal coaxial cylinders. The inner and outer cylinders, of radii r_i and r_o, respectively, are maintained at constant and uniform temperatures, T_i and T_o, respectively, with $T_o < T_i$. The porous medium, with porosity ε and permeability K, is saturated by an incompressible Newtonian fluid of kinematic viscosity ν, thermal expansion coefficient β and density ρ. The saturated porous medium is equivalent to an artificial fluid of heat capacity $(\rho c)^* = \varepsilon(\rho c)_f + (1-\varepsilon)(\rho c)_s$ and of thermal conductivity λ^*. The radii ratio $R = r_o/r_i$ characterizes the system's geometry for the 2D state. In order to simplify the formulation, several classical assumptions have been made.

(i) The Boussinesq approximation and Darcy's law are assumed to be valid.

(ii) The inertia terms and viscous dissipations are neglected.

(iii) The fluid is assumed to be in thermal equilibrium with the porous matrix.

A conformal transformation is used to shift from polar (r, ϕ) to cartesian coordinates $(X = \ln r, Y = \phi)$. The initial domain $[1, R] \times [0, \pi]$ thus becomes a rectangular domain $[0, \ln R] \times [0, \pi]$ (see Fig. 1).

In dimensionless form, the governing equations, formulated in terms of stream function ψ and temperature T, then read, for the steady 2D state

$$\nabla^2 \psi = Ra^* \exp(X)\left[\sin Y \frac{\partial T}{\partial X} + \cos Y \frac{\partial T}{\partial Y}\right] \quad (1)$$

$$\nabla^2 T = \frac{\partial T}{\partial X}\frac{\partial \psi}{\partial Y} - \frac{\partial T}{\partial Y}\frac{\partial \psi}{\partial X}. \quad (2)$$

The Rayleigh number of filtration appears in these equations

$$Ra^* = \frac{g\beta K(T_i - T_o)r_i(\rho c)_f}{\lambda^* \nu}.$$

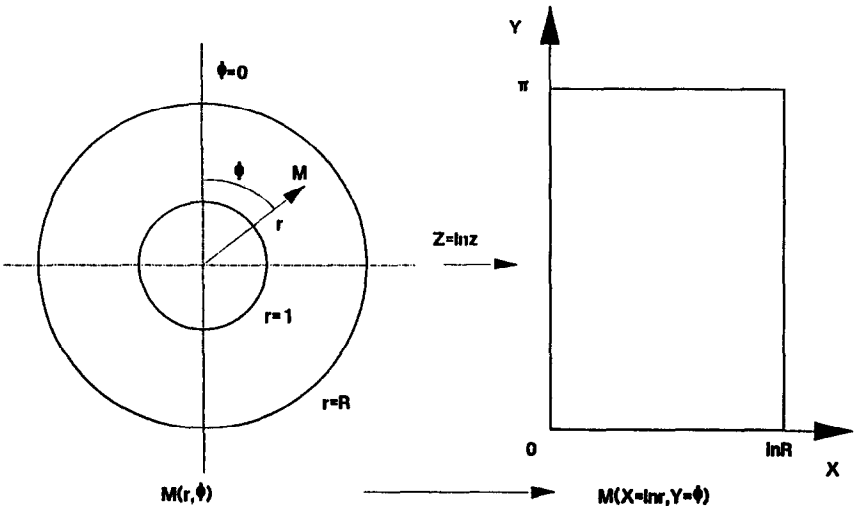

FIG. 1. Definition's scheme.

According to experimental results, we assume that the flow is symmetrical with respect to the vertical plane containing the cylinder's axis. The boundary conditions can then be summarized as follows:

$$\begin{cases} X=0: & T=1 \quad \psi=0 \,\forall\, Y & (3) \\ X=\ln R=\dfrac{1}{\alpha}: & T=0 \quad \psi=0 \,\forall\, Y & (4) \\ Y=0,\pi: & \dfrac{\partial T}{\partial Y}=0 \quad \psi=0 \,\forall\, X. & (5) \end{cases}$$

2.2. *Full Fourier–Galerkin approximation*

(a) *Formulation.* The stream function ψ and the temperature T are expanded into Fourier series in both, radial and azimuthal, directions

$$\begin{cases} \psi = \sum_{m=1}^{M} \sum_{n=1}^{N} a_{mn} \sin(m\pi\alpha X) \sin(nY) & (6) \\ T = 1-\alpha X + \sum_{m=1}^{M} \sum_{n=0}^{N} b_{mn} \sin(m\pi\alpha X) \cos(nY) & (7) \end{cases}$$

where the coefficients a_{mn} and b_{mn} are functions of the Rayleigh number and the radii ratio R. To deal with the nonlinear advection term in equation (2) a fictitious time τ is introduced and a transient form of energy equation (2′) is used

$$\frac{\partial T}{\partial \tau} = \nabla^2 T - \left(\frac{\partial T}{\partial X}\frac{\partial \psi}{\partial Y} - \frac{\partial T}{\partial Y}\frac{\partial \psi}{\partial X} \right). \qquad (2')$$

The Fourier series (equations (6) and (7)) are inserted into equations (1) and (2′) which in turn are projected on each Fourier basis function, $\sin(p\pi\alpha X) \times \sin(qY)$ and $\sin(p\pi\alpha X)\cos(qY)$ for the momentum and energy equations, respectively.

The coefficients b_{pq} and a_{pq} are solutions of a system of coupled, nonlinear, first-order in time differential equations.

(b) *2D multicellular flow analysis.* All the previous studies of this problem performed by the Fourier–Galerkin method used orders of approximation less than $M \times N = 20 \times 20$.

In order to test the accuracy of the Fourier–Galerkin spectral method, we focus our attention on the choice of M and N. Of course, it is not necessary to use high orders M, N for the representation of the unicellular flows, but when the bicellular, tricellular or multicellular flows are considered, higher orders of approximation are required, to capture the various expected boundary layers, appearing not only on both ends of the confined radial direction, but also in the azimuthal direction at the cell interfaces. Thus, orders of approximation up to 50×50 have been chosen to describe the flows corresponding to Rayleigh numbers ranging from 50 to 1000 and radii ratios of $2^{1/8}$, $2^{1/4}$, $2^{1/2}$ and 2.

Using the fast Fourier transform (FFT) to calculate the nonlinear term (**V grad** T) leads to a significant gain of CPU time. The time integration is performed following an exponential fitting scheme [15] which has been proved to be better than the classical Adams–Bashforth scheme used in our previous work [4].

Applied to the spectral formulation of the energy equation

$$\frac{db_{pq}}{d\tau} = -L(p,q)b_{pq} + N(p,q)$$

(L and N are respectively linear and nonlinear operators of the system), this exponential scheme reads

$$b_{pq}^{n+1} = b_{pq}^{n} - \{1-\exp[-L(p,q)\,d\tau]\}\left[b_{pq}^{n} - \frac{N^n(p,q)}{L(p,q)} \right]$$

where $N''(p, q)$ contains all the known quantities at time level $n\,d\tau$.

The convergence test is based on the global Nusselt number Nu_g^*

$$Nu_g^* = -\frac{\ln R}{\pi}\int_0^{\pi}\left.\frac{\partial T}{\partial r}\right|_{r=1} d\phi = 1 - \pi\sum_{m=1}^{M} mb_{m0}. \tag{8}$$

The convergence of the spectral coefficients is also considered.

For each pair (Ra^*, R) investigated the unicellular flow is obtained. For a given (Ra^*, R) bicellular, tricellular or multicellular flows are obtained by introducing various initial conditions if Ra^* is higher than a critical value which depends on R. Figures 2(a)–(c) show the different flow patterns for $Ra^* = 200$ and $R = 2$ and Fig. 3 shows the multicellular flow obtained for $Ra^* = 1000$ and $R = 2^{1/4}$. In Tables 1–3, the results of the computations for $R = 2$, $2^{1/2}$ and $2^{1/4}$ are summarized.

Let us consider the case $Ra^* = 200$, $R = 2$ and initial conditions which must induce a tricellular 2D flow. For the approximation $M \times N = 12 \times 12$ we indeed obtain a tricellular 2D flow with a global Nusselt number $Nu_g^* = 3.17$, a good convergence of the solution is observed. With the same initial conditions and $M \times N = 14 \times 14$, we obtain a unicellular flow with a global Nusselt number of 2.69. $M \times N = 16 \times 16$, oscillations occur in the computations and no steady state could be obtained.

With $M \times N = 20 \times 20$ the unicellular 2D flow is observed again and for $M \times N = 30 \times 30$; 40×40; 50×50 the flow is tricellular and the overall heat transfer is characterized by a global Nusselt number close to 3.

A similar behavior is found again for $R = \sqrt{2}$ and $2^{1/4}$. For Ra^* and R fixed and for identical initial conditions, a unicellular or bicellular or tricellular or multicellular flow can be obtained, depending only on orders of approximations.

The first conclusion to be drawn from these results is that orders of approximation higher than 50×50 must be chosen to represent the bicellular, tricellular and multicellular flows obtained for high Rayleigh numbers.

But is it enough to increase M and N to get good converged results? The stream function and temperature radial derivatives are expected to be non-periodic in the radial direction. Their Fourier coefficients should then follow a $1/M^2$ asymptotic decreasing law [16, 17], giving rise to very bad second-order radial derivative evaluations and to a Gibbs phenomenon in radial fluxes close to the radial boundaries. Such a well-known behavior is enhanced by the exp (X) function present in the equations to be solved. So, the full Fourier–Galerkin procedure leads to a mathematical problem which could be somewhat different from the original one and might well induce the observed puzzling results.

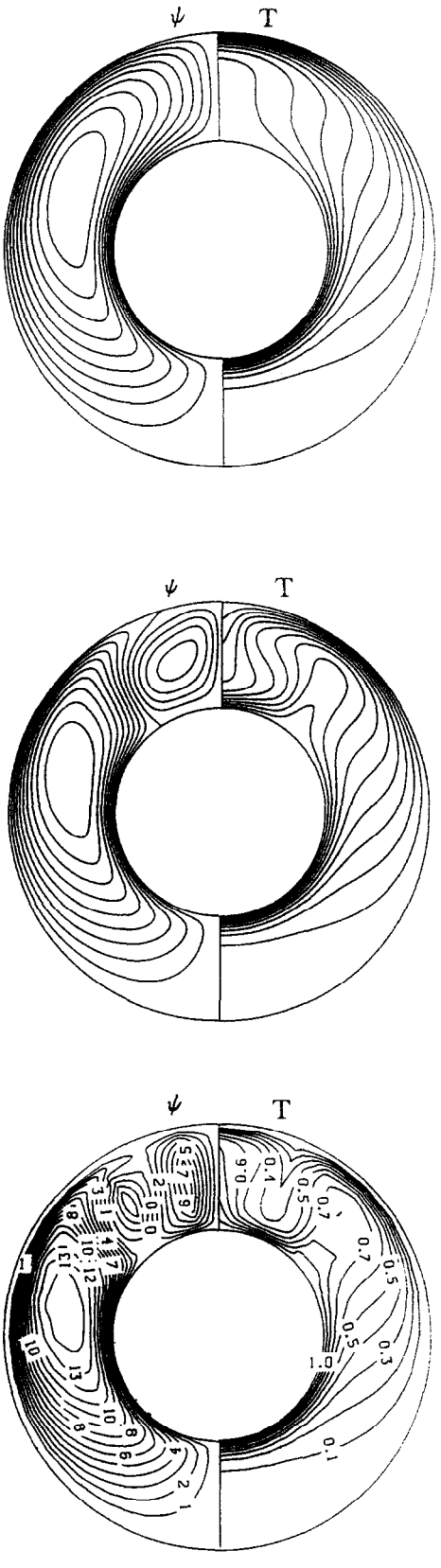

FIG. 2. (a) Isotherms and streamlines for $Ra^* = 200$, $R = 2$, unicellular flow. (b) Isotherms and streamlines for $Ra^* = 200$, $R = 2$, bicellular flow. (c) Isotherms and streamlines for $Ra^* = 200$, $R = 2$, tricellular flow.

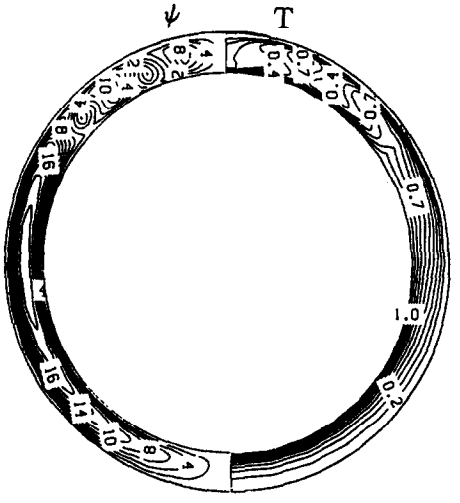

FIG. 3. Isotherms and streamlines for $Ra^* = 1000$, $R = 2^{1/4}$, multicellular flow.

(c) *Linear stability analysis.* A linear stability analysis of the multicellular 2D flows has been carried out with perturbations localized in the flow plane [18]. The basic motion has been numerically obtained with the Fourier–Galerkin method and orders of approximation up to $M \times N = 16 \times 16$.

Disturbance temperature and stream function have been expanded into Fourier series in both directions and with $M \times N = 16 \times 16$. Then these disturbances have been computed with the same algorithm that has been previously used to obtain the basic motion.

The cases $R = 2^{1/4}$, $2^{1/2}$ and 2 have been considered with Rayleigh numbers ranging from 50 to 1000. The computations made with these approximations (for the basic and the disturbance motions) do not allow us to find the results previously obtained by Himasekhar and Bau [6]. The discrepancy between these two studies might well be of numerical origin.

Table 1. Fourier–Galerkin method for $R = 2$. CI, initial conditions. Type I, for unicellular flows: $a_{ij} = 0$, $b_{ij} = 0.001\ \forall i, j$. Type II, for bicellular flows: $a_{ij} = 0$, all $b_{ij} = 0$ except $b_{13} = -0.1$, $b_{14} = 0.1$, $b_{15} = -0.1$. Type III, for tricellular flows: $a_{ij} = 0$, all $b_{ij} = 0$ except $b_{16} = -0.2$, $b_{17} = 0.2$, $b_{18} = -0.2$, $b_{19} = 0.2$

Ra^*	CI	M	N	Nu_g^*	Flow
120	I	10	10	2.056	Unicellular
120	I	50	50	2.050	Unicellular
120	II	16	16	2.260	Bicellular
120	II	30	30	2.266	Bicellular
120	III	30	30	2.050	Unicellular
120	III	40	40	2.050	Unicellular
200	I	12	12	2.69	Unicellular
200	I	30	30	2.68	Unicellular
200	II	30	30	2.91	Bicellular
200	II	40	40	2.90	Bicellular
200	II	50	50	2.90	Bicellular
200	III	12	12	3.17	Tricellular
200	III	14	14	2.69	Unicellular
200	III	16	16	2.97–3.03	Tricellular
200	III	20	20	2.685	Unicellular
200	III	30	30	3.00	Tricellular
200	III	40	40	2.968	Tricellular
200	III	50	50	2.968	Tricellular
300	I	30	30	3.287	Unicellular
300	II	30	30	3.37–3.73	Bicellular
300	II	40	40	3.45–3.57	Bicellular
300	II	50	50	3.48–3.56	Bicellular
300	III	30	30	3–3.70	Tricellular
300	III	40	40	3.50–3.60	Tricellular

Table 2. Fourier–Galerkin method for $R = 2^{1/2}$

Ra^*	CI	M	N	Nu_g^*	Flow
500	I	10	10	1.913	Unicellular
500	I	20	20	2.42	Tricellular
500	I	30	30	2.40	Tricellular
500	I	40	40	2.41	Tricellular
500	II	16	16	2.21	Bicellular
500	II	30	30	2.26	Bicellular
500	II	40	40	2.2–2.40	Multicellular
500	III	30	30	2.40	Tricellular
500	III	40	40	2.40	Tricellular
1000	I	10	10	2.75	Unicellular
1000	I	12	12	3.51	Tricellular
1000	I	16	16	3.4–3.6	Tricellular

2.3. *Collocation–Chebyshev approximation*

(a) *Formulation and numerical procedure.* In this new development, we adopt a Fourier–Galerkin approximation for the periodic ϕ-direction and a collocation–Chebyshev approximation in the confined r-direction.

The stream function ψ and the temperature T are then expanded as follows:

$$\begin{cases} \psi = \sum_{n=1}^{N} f_n(X) \sin(nY) & (9) \\ T = 1 - \alpha X + \sum_{n=0}^{N} g_n(X) \cos(nY). & (10) \end{cases}$$

Table 3. Fourier–Galerkin method for $R = 2^{1/4}$

Ra^*	CI	M	N	Nu_g^*	Flow
250	I	16	16	1.027	Unicellular
250	I	30	30	1.049	Multicellular
250	II	16	16	1.027	Unicellular
250	II	20	20	1.027	Unicellular
250	II	30	30	1.048	Multicellular
250	III	16	16	1.027	Unicellular
250	III	30	30	1.050	Multicellular
250	III	40	40	1.051	Multicellular
500	I	16	16	1.303	Multicellular
500	II	16	16	1.310	Multicellular
500	III	16	16	1.303	Multicellular
500	I	30	30	1.318	Tricellular
500	II	40	40	1.320	Tricellular
500	III	40	40	1.397	Multicellular
1000	I	16	16	1.749	Tricellular
1000	II	16	16	1.559	Bicellular
1000	III	16	16	1.749	Tricellular
1000	II	40	40	2.060	Multicellular

Expansions (9) and (10) are inserted in equations (1) and (2), which are then properly projected on the Fourier basis functions.

The functions f_p and g_p are thus solutions of the second-order differential system

$$\begin{cases} f_p''(x) - \dfrac{p^2}{4\alpha^2} f_p(x) = F_p(x) \\ F_p = F_p(g'_{p+1}, g'_{p-1}, g_{p+1}, g_{p-1}) \end{cases} \quad (11)$$

$$\begin{cases} g_p''(x) - \dfrac{p^2}{4\alpha^2} g_p(x) = G_p(x) \\ G_p = G_p(f_p, f_{p+n}, f_{p-n}, g_n, g'_n) \end{cases} \quad (12)$$

where $x = 2\alpha X - 1$; $x \in [-1, +1]$.

The boundary conditions for the functions $f_p(x)$ and $g_p(x)$ are

$$f_p(-1) = f_p(+1) = 0$$

and

$$g_p(-1) = g_p(+1) = 0 \; \forall p.$$

System (11) and (12) is discretized using the collocation–Chebyshev method with the commonly used Gauss–Lobatto points $\{x_j = \cos[j\pi/(M-1)]$ $j = 0 \ldots M-1\}$.

The functions $f_p(x)$ and $g_p(x)$ are expanded in a truncated series of Chebyshev polynomials

$$f_p(x) = \sum_{m=1}^{M} \xi_{mp} T_{m-1}(x)$$

and

$$g_p(x) = \sum_{m=1}^{M} \theta_{mp} T_{m-1}(x)$$

where $T_k(x) = \cos(k \arccos x)$.

Let us recall that the density of the Gauss–Lobatto points is increased near the boundaries $x = -1$ (i.e. $r = 1$) and $x = +1$ (i.e. $r = R$), ensuring an accurate description of the radial boundary layers.

The linear system coming from equations (11) (and (12)) is full and can be efficiently solved, in NM^2 operations, by a diagonalization procedure of the Chebyshev second-order derivative operator, D^{*2}, properly modified to take into account the boundary conditions [19]. The diagonalization itself, performed once for all in a preprocessing step storage, is required only for the $(M-2)$ eigenvalues and $(M-2)^2$ matrices (the eigenvector matrix and its inverse).

The transient form (equation (12′)) of equation (12) is used to ensure the scheme stability

$$\frac{\partial[g_p]}{\partial t} = [D^{*2} - k^2 I][g_p] - [G_p] \quad (12')$$

where

$$[g_p] = \begin{bmatrix} g_p(x_1) \\ g_p(x_{M-2}) \end{bmatrix}$$

I is the unity matrix and $k^2 = p^2/4\alpha^2$. The time integration is performed with the exponential fitting scheme that has been described in Section 2.2(a).

Table 4. Comparison between Fourier–Galerkin and collocation–Chebyshev methods for unicellular flows

Ra^*	R	M	N	Nu_g^* (Chebyshev)	Nu_g^* (Galerkin)
50	$2^{1/8}$	10	8	1.0000646	1.0000647
100	$2^{1/8}$	10	8	1.000259	1.000258
200	$2^{1/8}$	10	8	1.001033	1.001030
500	$2^{1/8}$	10	8	1.006427	1.006425
50	$2^{1/4}$	10	8	1.0011	1.0011
100	$2^{1/4}$	10	8	1.0045	1.0045
200	$2^{1/4}$	10	8	1.0177	1.0177
500	$2^{1/4}$	10	8	1.1021	1.1021
1000	$2^{1/4}$	10	8	1.3299	1.3298
50	$2^{1/2}$	10	8	1.02047	1.02054
200	$2^{1/2}$	10	8	1.2650	1.2658
500	$2^{1/2}$	16	10	1.9137	1.9131
50	2	16	8	1.343	1.344
120	2	16	16	2.053	2.056
200	2	30	30	2.683	2.685
300	2	30	30	3.309	3.287

In order to analyze the spectral convergence of this new expansion, the coefficients θ_{mn} are calculated after each computation using the matrix $[C]$ representing the transformation from the physical space to Chebyshev transform space [16].

(b) *Results and comparison with Fourier–Galerkin method.* To test the validity of this new numerical scheme, we first compare the results obtained with the collocation–Chebyshev method and Fourier–Galerkin method for the case of unicellular flows (Table 4).

For all the radii ratios ($R = 2^{1/8}$, $2^{1/4}$, $\sqrt{2}$, 2) and all the Rayleigh numbers considered in the computations, the numerical results are in good agreement.

Then, we focus our attention on the case $R = 2$ and the representation of the bicellular and tricellular flows. For the case $Ra^* = 200$ and $R = 2$ the spectral accuracy of the two methods is studied very carefully. On Figs. 4(a) and 5(a) the evolutions of the spectral coefficients $b_{m0}(m)$ (for the Fourier–Galerkin method) and $\theta_{m0}(m)$ (for the collocation–Chebyshev method) are compared for the bicellular and tricellular flows. For both cases, we observe that the spectral convergence upon x (i.e. r) is better for the collocation–Chebyshev method than for the Fourier–Galerkin method. For the approximation of 30×30, the spectral coefficients θ_{mn} decrease until 10^{-9} while the coefficients b_{mn} only decrease until 10^{-5}.

If we now examine the spectral convergence of the two methods upon ϕ, Figs. 4(b) and 5(b) show a similar evolution for $\theta_{1n}(n)$ and $b_{1n}(n)$. Let us note that for $N = 30$, the spectral convergence on ϕ is not sufficient, the lower coefficients are between 10^{-3} and 10^{-4} for the two methods.

As might be expected, the spectral accuracy of the collocation–Chebyshev method to describe the solution along the r-coordinate is better than the Fourier–Galerkin method. Due to the evolutions of the co-

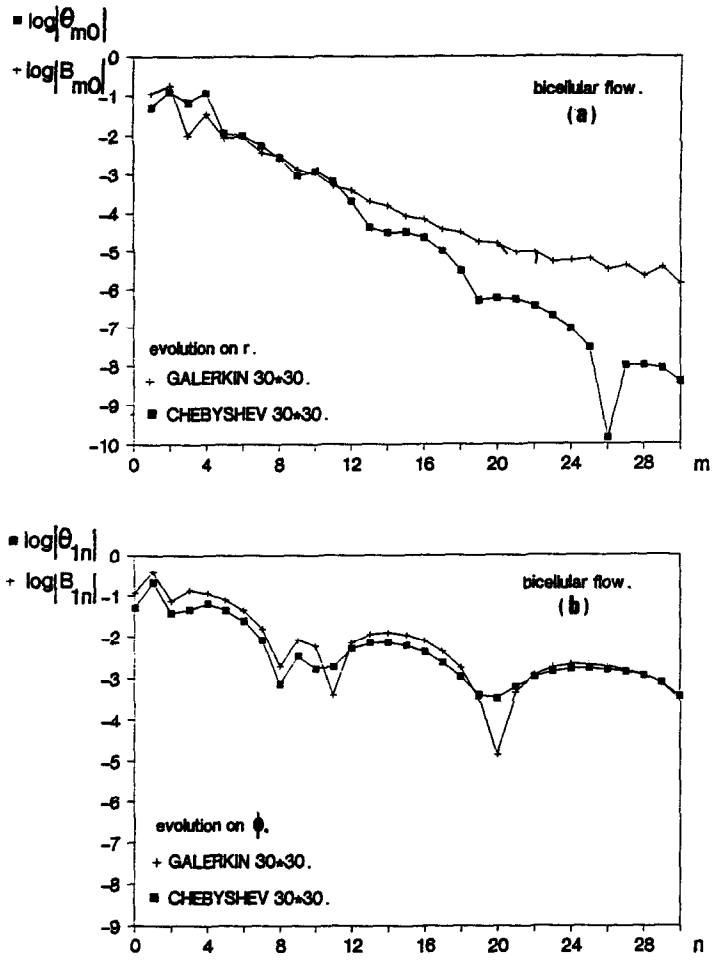

FIG. 4. Comparison between Fourier–Galerkin and collocation–Chebyshev spectral coefficients for bicellular flow ($M \times N = 30 \times 30$), $Ra^* = 200$, $R = 2$: (a) variation with m for $n = 0$; (b) variation with n for $m = 1$.

efficients θ_{mn} as functions of m and n we decided to carry on our computations with the collocation–Chebyshev method limiting the order of approximation M between 20 and 30 and increasing the order N up to 80 (Table 5).

For $Ra^* = 200$ ($R = 2$) Figs. 6(a) and (b) show the evolution of $\theta_{1n} = \mathscr{F}(n)$ for the approximation $M \times N = 20 \times 80$ and the comparison with the approximation 30×30. Both bicellular and tricellular flows are considered. For the bicellular flow the spectral coefficients decrease regularly after $n = 30$ to reach the value of 5×10^{-7} for $n = 80$. For the tricellular flow the coefficients also decrease after $n = 30$ but with numerous oscillations.

The authors therefore believe that orders of approximation higher than $N = 80$ are required to describe, with a good accuracy, all the boundary layers which exist in the azimuthal direction for the tricellular flows and of course for the multicellular flows.

To complete our study, we also analyzed the convergence of the computations based on the global Nusselt number Nu_g^* ($Nu_g^* = 1 - 2g_0'(x = -1)$). On Figs. 7(a) and (b), the curves $Nu_g^* = f(t)$ have been plotted for $Ra^* = 200$, $R = 2$ and for the bicellular and tricellular flows (computed with the collocation–Chebyshev method $M \times N = 20 \times 80$). We obtained, with about 2200 iterations, a good convergence upon the Nusselt number. For the case $Ra^* = 300$ and $R = 2$ we need more than 5000 iterations (for $M \times M = 20 \times 80$) to ensure a good convergence: the CPU time becomes higher than 15 min on IBM 3090 VF (with vectorized code).

3. EXPERIMENTAL STUDY

3.1. *Experimental apparatus and Christiansen effect*

In order to visualize the multicellular 2D flows, experiments have been realized with a cell (Fig. 8) corresponding to a radii ratio of $R = 2$. The inner and outer cylinders have a length $L = 20$ mm, the radius value is 40 mm for the inner cylinder and 80 mm for the outer cylinder. Both cylinders are in copper and they are kept at constant temperature with circulating

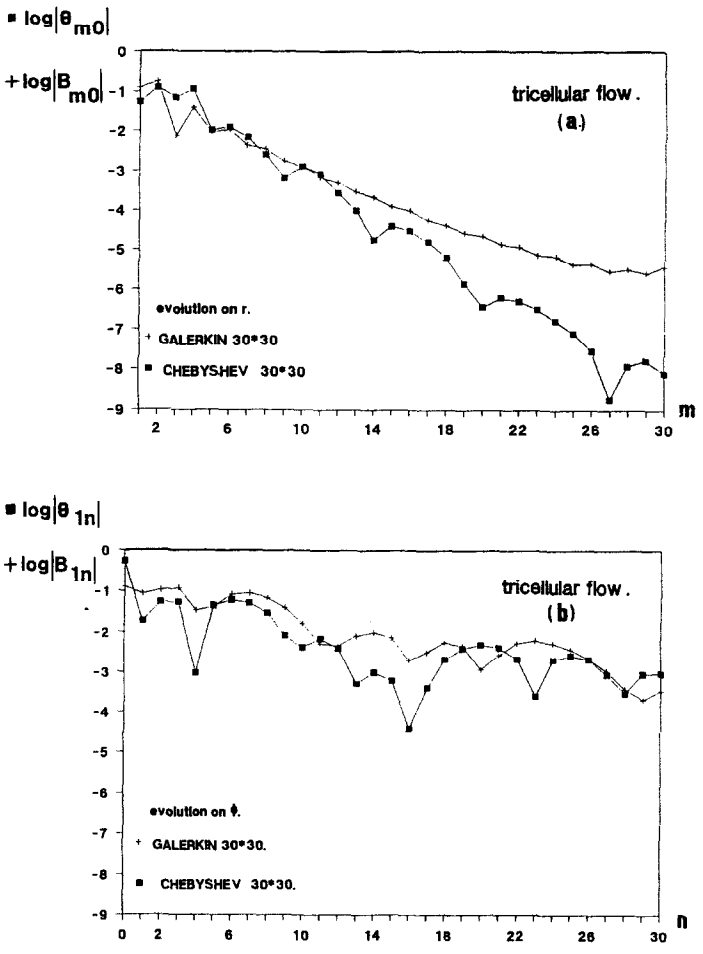

FIG. 5. Comparison between Fourier–Galerkin and collocation–Chebyshev spectral coefficients for tricellular flow ($M \times N = 30 \times 30$), $Ra^* = 200$, $R = 2$: (a) variation with m for $n = 0$; (b) variation with n for $m = 1$.

Table 5. Collocation–Chebyshev method for $R = 2$. CI, I, II, III, initial conditions for unicellular, bicellular and tricellular flows respectively expressed in terms of $f_p(x_j)$ and $g_p(x_j)$

Ra^*	CI	M	N	Nu_g^*	Flow
120	I	30	30	2.052	Unicellular
120	II	30	30	2.261	Bicellular
120	III	20	80	2.050	Unicellular
200	I	30	30	2.683	Unicellular
200	I	20	80	2.684	Unicellular
200	II	30	30	2.913	Bicellular
200	II	20	80	2.907	Bicellular
200	III	16	16	2.5–3.12	Tricellular
200	III	20	20	2.683	Unicellular
200	III	30	30	3.001	Tricellular
200	III	40	40	2.995	Tricellular
200	III	20	80	3.000	Tricellular
300	I	30	30	3.309	Unicellular
300	I	20	80	3.310	Unicellular
300	II	30	30	3.30–3.70	Bicellular
300	II	40	40	3.33–3.58	Bicellular
300	II	20	80	3.55–3.70	Bicellular
300	III	30	30	3.42–3.70	Tricellular
300	III	40	40	3.45–3.78	Tricellular
300	III	20	80	3.310	Unicellular

water. The Christiansen effect is used to visualize the thermal field for different Rayleigh numbers. The theory of the Christiansen effect has been developed by Christiansen [20], Raman [21], Clarke [22] and more recently by Klarsfeld [23].

For our experiments the porous matrix is made of small particles of special glass (diameter of 1200 μm) saturated with an organic liquid: chlorobenzene. The solid phase optical refractive index, n_S, does not vary with the temperature while the fluid phase one, n_F, varies appreciably with the temperature (Fig. 9). If the cell is isothermal, only the rays of wavelength λ_c with $n_S(\lambda_c) = n_F(\lambda_c)$ can cross it; the rays of wavelength different from λ_c are diffused: the cell is like a filter with a bandwidth centered around λ_c. When natural convection appears, the nonisothermal cell is like a set of elementary filters, the isothermal lines, which are iso-optical index lines as well, being viewed as isochrom lines. This optical technique can only be used for the visualization of 2D phenomena. If the flow is 3D, the light is completely diffused by the successive slabs which constitute the medium and no

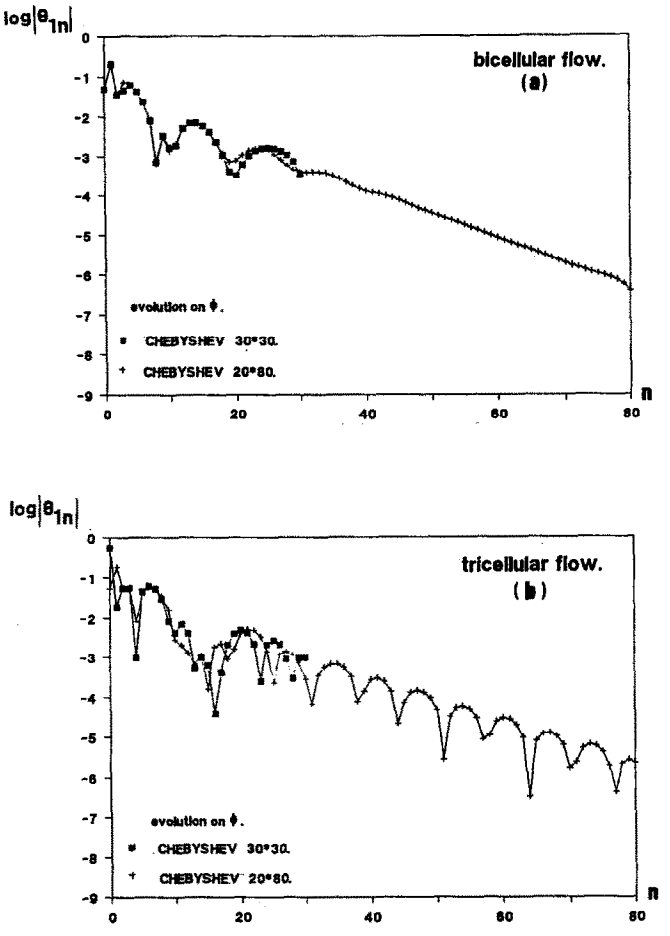

FIG. 6. Evolution of spectral coefficients as a function of n for collocation–Chebyshev method and different values of N ($Ra^* = 200$, $R = 2$): (a) bicellular flow; (b) tricellular flow.

isotherm lines can be observed (the photographs are dark).

The visualization is realized with discontinuous spectrum light-sources (Hg–Cd) (Fig. 10). In the experiments, the cell is lit with parallel light, and an exit diaphragm stops the diffused light and a photograph of the thermal field is taken.

The vertical glasses are isolated with polystyrene. Special care must be taken to fill the cell and to obtain a homogeneous medium. For each Rayleigh number, the steady state is reached in a few hours. In these experiments, we have been only concerned with the visualization of the thermal field, no heat transfer rate measurements have been carried out.

3.2. *Results and discussion*

Two series of experiments have been made in order to prove the physical significance of the multicellular flows obtained with the numerical simulations.

In the first series of experiments the cell has been divided in two equal parts of length $L = 9.5$ mm in order to prevent 3D perturbations from developing.

The results obtained in this case are presented on photographs of Fig. 11 and correspond to the visualization of thermal fields for Rayleigh numbers of 59 (photo No. 1), 109 (photo No. 2) and 213 (photo No. 3) (each Rayleigh number is evaluated with an error $\Delta Ra^* = 5$). Whatever the Rayleigh number is, a unicellular flow, symmetrical with respect to a vertical plane including the cylinder's axis, is observed. As Ra^* increases, the convective phenomena become more important and the isotherms are especially distorted in the upper part of the cell. (Note that with the Christiansen effect the blue color stands for high temperatures and the red color for low temperatures.) These results agree well with the numerical computations. (The photograph $Ra^* = 213$ (Fig. 11) can be compared to Fig. 2(a), which corresponds to $Ra^* = 200$, with a good approximation due to the experimental error on the evaluation of Ra^*.)

In the second series of experiments the length of the cell was $L = 20$ mm. The results obtained in this case are particularly interesting; they are presented in the photographs of Fig. 12. In this case we observe that when the Rayleigh number increases up to 250, the 2D unicellular flow becomes 3D in the upper part of

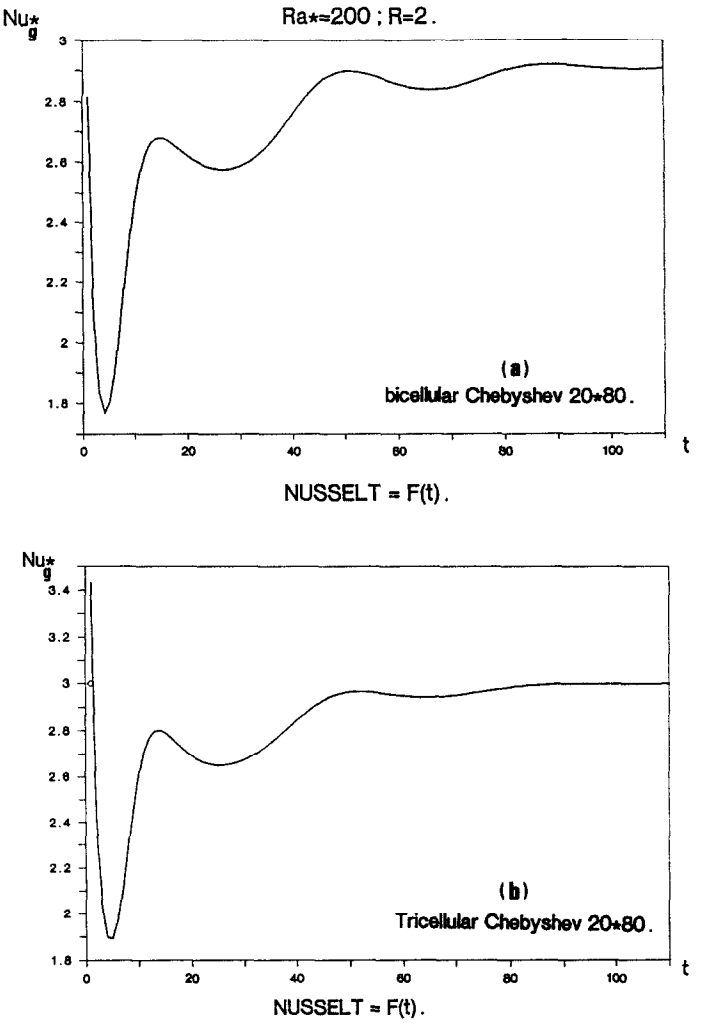

FIG. 7. Evolution of Nusselt number as a function of time t for collocation–Chebyshev method ($M \times N = 20 \times 80$), $Ra^* = 200$, $R = 2$: (a) bicellular flow; (b) tricellular flow.

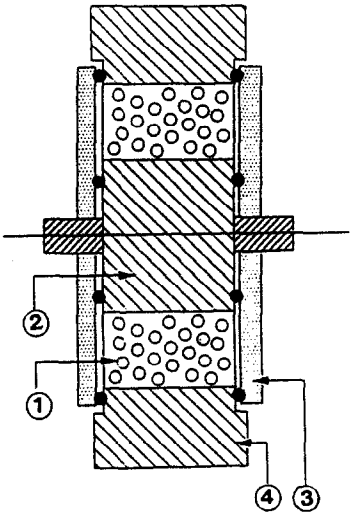

FIG. 8. Experimental cell: 1, porous medium; 2, inner cylinder; 3, glasses; 4, outer cylinder.

the annular region and still remains 2D in the lower part. These 3D perturbations lead to the apparition of a dark region which can be observed on the photograph corresponding to $Ra^* = 338$ (photo No. 6). The other photographs of Fig. 12 have been taken

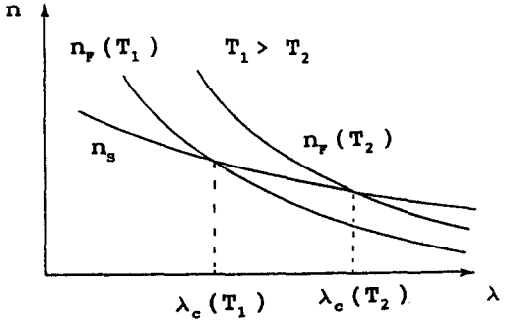

FIG. 9. Variation of Christiansen wavelength λ_c with temperature.

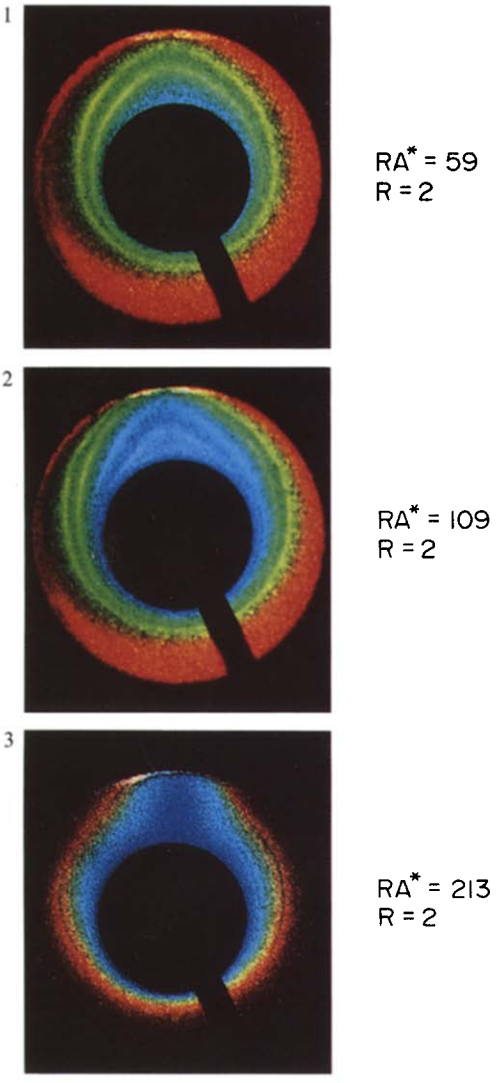

FIG. 11. Thermal fields visualizations, unicellular flows for $R = 2$: photo No. 1, $Ra^* = 59$; photo No. 2, $Ra^* = 109$; photo No. 3, $Ra^* = 213$.

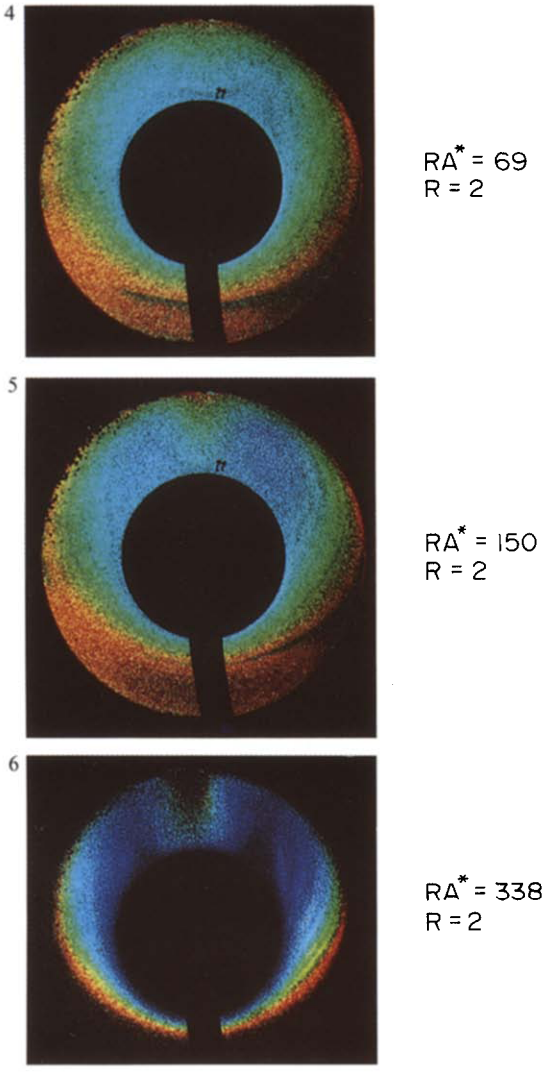

FIG. 12. Thermal fields visualizations, bicellular flows for $R = 2$: photo No. 4, $Ra^* = 69$; photo No. 5, $Ra^* = 150$; photo No. 6, $Ra^* = 338$.

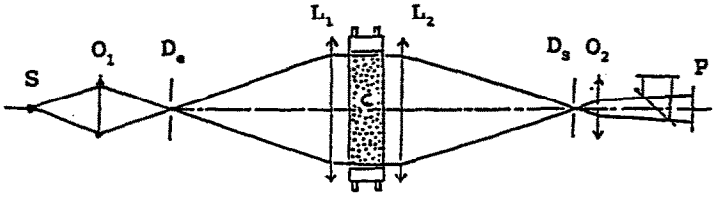

FIG. 10. Visualization of thermal fields, optical scheme: S, light source Cd–Hg; C, cell; O_1, O_2, L_1, L_2, lenses; P, photographic film; D_e, D_s, entrance and exit diaphragm.

during the cooling phase. The difference of temperature between the two cylinders has been progressively reduced. (Each photograph has been taken 1 h after the flow stabilization.) The flow pattern becomes 2D again on all the annuli, which corresponds to the disappearance of the dark region in the upper part of the cell and the appearance of the isochrom lines.

The photograph of $Ra^* = 150$ (photo No. 5) shows a 2D bicellular flow pattern, symmetrical with respect to the vertical axis, with a counter-rotating cell between $\phi = 0°$ and $\phi \simeq 30°$. This flow is similar to the one numerically obtained on Fig. 2(b). The 2D bicellular flow still remains for $Ra^* = 69$ (photo No. 4) and the unicellular flow is again observed for Rayleigh number lower than 65 (± 5). These results agree with the stability analysis developed by ref. [6]. However, the experimental procedure used does not allow us to conclude that these observed 2D bicellular structures are stable. It is possible that these structures turn out to be 2D unicellular flows after a few hours. Actually, other experiments are realized in order to specify, with more details, the onset of bicellular and multicellular flows.

4. CONCLUDING REMARKS

Natural convection in horizontal cylindrical porous annuli has been studied numerically and experimentally. We focus our attention on the characterization of the multicellular 2D flows. These flows have been calculated using both collocation–Chebyshev and full Fourier–Galerkin methods.

Computations have been conducted for Rayleigh numbers ranging from 50 to 1000 and radii ratios of $2^{1/8}$, $2^{1/4}$, $2^{1/2}$ and 2. In case of unicellular flows, the results obtained by the two methods are in good agreement.

For the description of the bicellular, tricellular and multicellular flows the collocation–Chebyshev method presents a better spatial radial accuracy. For the studied cases ($Ra^* = 120$, 200, 300, $R = 2$ bicellular and tricellular flows) less than 30 collocation points are necessary to obtain a good accuracy in the r-direction while 30 Fourier components are not sufficient to obtain the same accuracy with the Fourier–Galerkin method. Concerning the convergence in the azimuthal direction, it is shown that almost 80 terms in the Fourier series are required in both methods. The authors believe that a stability analysis performed with basic flows obtained through the collocation–Chebyshev method at high orders will give further details on the transition between the 2D multicellular flows.

The experimental study allows us to observe the bicellular 2D structures; however, more experiments are needed to prove the physical existence of these flows. Anyway the transition from unicellular to multicellular flows depends strongly on the initial experimental conditions.

Acknowledgements—The authors would like to acknowledge the CNUSC (National Center of Computations of Montpellier) for its financial support, the laboratory L.E.P.T., E.N.S.A.M. of Bordeaux I where some experiments have been realized and the laboratory F.A.S.T., Orsay–Paris VI where some computations have been made.

REFERENCES

1. J. P. Caltagirone, Thermoconvective instabilities in a porous medium bounded by two concentric horizontal cylinders, *J. Fluid Mech.* **76**, 337–362 (1976).
2. P. J. Burns and C. L. Tien, Natural convection in porous medium bounded by concentric spheres and horizontal cylinders, *Int. J. Heat Mass Transfer* **22**, 929–939 (1979).
3. A. Mojtabi, D. Ouazar and M. C. Charrier-Mojtabi, An efficient finite element code for 2D steady state in porous annular, *Proc. Int. Conf. Numerical Methods for Thermal Problems*, Montreal, Vol. 5, Part 1, pp. 644–654 (1987).
4. M. C. Charrier-Mojtabi and J. P. Caltagirone, Numerical simulation of natural convection in an annular porous layer by spectral method, *Proc. Ist Int. Conf. of Numerical Methods for Non-linear Problems*, Swansea, pp. 821–828 (1980).
5. Y. F. Rao, K. Fukuda and S. Hasegawa, Steady and transient analysis of natural convection in a horizontal porous annulus with Galerkin method, *J. Heat Transfer* **109**, 919–927 (1987).
6. K. Himasekhar and H. H. Bau, Two-dimensional bifurcation phenomena in thermal convection in horizontal concentric annuli containing saturated porous media, *J. Fluid Mech.* **187**, 267–300 (1988).
7. R. Echigo, S. Hasegawa, S. Tottori, H. Shimomura and Y. Okamoto, An analysis on the radiative and free convective heat transfer in a horizontal annulus with permeable insulator, *Proc. 6th Int. Heat Transfer Conf.*, Vol. 3, pp. 385–390 (1978).
8. H. H. Bau, Thermal convection in a horizontal eccentric annulus containing a saturated porous medium—an extended perturbation expansion, *Int. J. Heat Mass Transfer* **27**, 2277–2287 (1984).
9. K. Himasekhar and H. H. Bau, Large Rayleigh number

convection in a horizontal eccentric annulus containing saturated porous media, *Int. J. Heat Mass Transfer* **29,** 703–712 (1986).
10. K. Fukuda, Y. Takuta and S. Hasegawa, Three-dimensional natural convection in a porous medium between concentric inclined cylinders, ASME, Orlando, U.S.A. (1981).
11. M. C. Charrier-Mojtabi, A. Mojtabi and J. P. Caltagirone, Three dimensional convection in a horizontal porous layer, *Euromech. 138*, pp. 75–77, Karlsruhe (1981).
12. Y. F. Rao, K. Fukuda and S. Hasegawa, A numerical study of three dimensional natural convection in a horizontal porous annulus with Galerkin method, *Int. J. Heat Mass Transfer* **31,** 695–707 (1988).
13. M. Cloupeau and S. Klarsfeld, Visualization of thermal fields in saturated porous media by Christiansen effect, *Appl. Optics* **12,** 198–204 (1973).
14. H. H. Bau, G. McBlane and I. Saferstein, Numerical simulation of thermal convection in an eccentric annulus containing porous media, ASME 83 WA/HT 34 (1983).
15. J. P. Caltagirone and P. Fabrie, Natural convection in porous media at high Rayleigh numbers; Part I. Darcy model, Congrès de Mécanique, I.U.T.A.M., Grenoble, France (1988).
16. D. Gottlieb and S. A. Orzag, *Numerical Analysis of Spectral Methods: Theory and Applications*. Springer, Berlin (1987).
17. C. Canuto, M. Y. Hussaini, T. A. Zang and A. Quarteroni, *Spectral Methods in Fluids Dynamics*. Springer, Berlin (1988).
18. M. C. Charrier-Mojtabi, Stability analysis of multicellular free convection flows in an annular porous layer, *Proc. Int. Forum Mathematical Modelling of Processes in Energy Systems*, Sarajevo, Yugoslavia (1989).
19. P. Haldenwang, G. Labrosse, S. Abboudi and M. Deville, Chebyshev 3-D spectral and 2-D pseudo spectral solvers for the Helmholtz equation, *J. Comp. Phys.* **55,** 277–290 (1984).
20. C. Christiansen, Untersuchungen uber die optichen eigenschaften von fein vertheilten körpen, *Ann. Phys.* **23,** 298–306 (1884).
21. C. V. Raman, The theory of the Christiansen experiment. *Proc. Ind. Acad. Sci.* **29,** 381–390 (1949).
22. R. H. Clarke, A theory for Christiansen filter, *Appl. Optics* **7,** 861–868 (1968).
23. S. Klarsfeld, Etude de la convection naturelle dans les milieux poreux, Thesis, University of Paris VI (1970).

ETUDE NUMERIQUE ET EXPERIMENTALE DES ECOULEMENTS MULTICELLULAIRES DE CONVECTION NATURELLE EN ESPACE ANNULAIRE POREUX

Résumé—On présente une étude numérique et expérimentale de la convection naturelle bidimensionnelle en espace annulaire poreux horizontal. L'écoulement, décrit par les équations de Darcy–Boussinesq, est obtenu par deux méthodes numériques différentes à savoir la méthode de Fourier–Galerkin et la méthode de collocation–Chebyshev. La précision spectrale des deux méthodes est comparée. Les résultats numériques montrent que la méthode de collocation–Chebyshev permet une meilleure description des écoulements dans la direction radiale. Une étude expérimentale, utilisant l'effet Christiansen pour la visualisation des champs thermiques, a permis de mettre en évidence, pour la première fois, l'existence physique d'écoulements bicellulaires bidimensionnels trouvés par voie numérique.

NUMERISCHE UND EXPERIMENTELLE UNTERSUCHUNG DER MULTIZELLULAREN FREIEN KONVEKTION IN EINEM PORÖSEN RINGRAUM

Zusammenfassung—Über die numerische und experimentelle Untersuchung zweidimensionaler freier Konvektionsströmungen in einem gesättigten porösen horizontalen Ringraum wird berichtet. Die Strömung wird mit Hilfe zweidimensionaler Darcy–Boussinesq Gleichungen beschrieben, welche mit Hilfe zweier verschiedener numerischer Methoden gelöst werden. Zur Anwendung kommt die Fourier–Galerkin Methode und für hohe Näherung die Collocation–Chebyshev Methode. Die spektrale Genauigkeit der beiden Verfahren wird verglichen. Die numerischen Berechnungen zeigen, daß die Collocation–Chebyshev Methode genauere Ergebnisse liefert, insbesondere bei der Beschreibung der Grenzschicht am inneren und äußeren Zylinder. Experimentelle Untersuchungen, bei denen das Temperaturfeld mit Hilfe der Methode nach Christiansen sichtbar gemacht wurde, zeigen bizellulare zweidimensionale Strukturen. Diese Strukturen wurden bisher noch nie in konzentrischen Ringräumen mit Hilfe des Christiansen-Effekts beobachtet, sie stimmen gut mit den numerischen Ergebnissen überein.

ЧИСЛЕННОЕ И ЭКСПЕРИМЕНТАЛЬНОЕ ИССЛЕДОВАНИЕ МНОГОЯЧЕНИСТЫХ СВОБОДНОКОНВЕКТИВНЫХ ТЕЧЕНИЙ В КОЛЬЦЕВОМ СЛОЕ ПОРИСТОГО МАТЕРИАЛА

Аннотация—Численно и экспериментально исследуются свободноконвективные двумерные течения в горизонтальном кольцевом слое насыщенного пористого материала. Течение жидкости, описываемое двумерными уравнениями Дарси–Буссинеска, определяется двумя различными приближенными методами, а именно, методом Фурье–Галеркина и Чебышевским методом коллокаций для приближений высокого порядка. Сравнивается спектральная точность обоих методов. Численные результаты свидетельствуют о том, что метод коллокаций является более точным, особенно при описании пограничных слоев, формирующихся у внутреннего и внешнего цилиндров. Экспериментальное исследование с использованием эффекта Кристиансена для висуализации тепловых полей показывает наличие двухячеистых двумерных структур. Эти структуры, никогда ранее не наблюдавшиеся в случае концентрических цилиндров посредтвом эффекта Кристиансена, хорошо согласуются с численными результатами.